

# Chemically Stable Multilayered Covalent Organic Nanosheets from Covalent Organic Frameworks via Mechanical Delamination

Suman Chandra,<sup>†</sup> Sharath Kandambeth,<sup>†</sup> Bishnu P. Biswal,<sup>†</sup> Binit Lukose,<sup>‡</sup> Shrikant M. Kunjir,<sup>§</sup> Minakshi Chaudhary,<sup>†</sup> Ravichandar Babarao,<sup>||</sup> Thomas Heine,<sup>‡</sup> and Rahul Banerjee<sup>\*,†</sup>

<sup>†</sup>Physical/Materials Chemistry Division, CSIR-National Chemical Laboratory, Dr. Homi Bhabha Road, Pune 411 008, India

<sup>‡</sup>Center for Functional Nanomaterials, School of Engineering and Science, Jacobs University Bremen, Research III, Room 61, Campus Ring 1, Bremen 28759, Germany

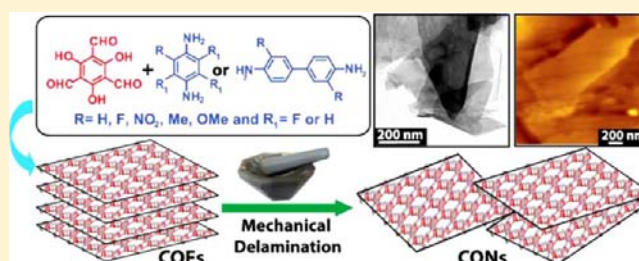
<sup>§</sup>Central NMR Facility, CSIR-National Chemical Laboratory, Dr. Homi Bhabha Road, Pune 411 008, India

<sup>||</sup>Materials Science and Engineering Division, Commonwealth Scientific and Industrial Research Organisation (CSIRO), Clayton, Victoria 3168, Australia

## Supporting Information

**ABSTRACT:** A series of five thermally and chemically stable functionalized covalent organic frameworks (COFs), namely, TpPa-NO<sub>2</sub>, TpPa-F<sub>4</sub>, TpBD-(NO<sub>2</sub>)<sub>2</sub>, TpBD-Me<sub>2</sub>, and TpBD-(OMe)<sub>2</sub> were synthesized by employing the solvothermal aldehyde-amine Schiff base condensation reaction. In order to complete the series, previously reported TpPa-1, TpPa-2, and TpBD have also been synthesized, and altogether, eight COFs were fully characterized through powder X-ray diffraction (PXRD), Fourier transform IR (FT-IR) spectroscopy, <sup>13</sup>C solid-state NMR spectroscopy, and thermogravimetric analysis.

These COFs are crystalline, permanently porous, and stable in boiling water, acid (9 N HCl), and base (3 N NaOH). The synthesized COFs (all eight) were successfully delaminated using a simple, safe, and environmentally friendly mechanical grinding route to transform into covalent organic nanosheets (CONs) and were well characterized via transmission electron microscopy and atomic force microscopy. Further PXRD and FT-IR analyses confirm that these CONs retain their structural integrity throughout the delamination process and also remain stable in aqueous, acidic, and basic media like the parent COFs. These exfoliated CONs have graphene-like layered morphology (delaminated layers), unlike the COFs from which they were synthesized.



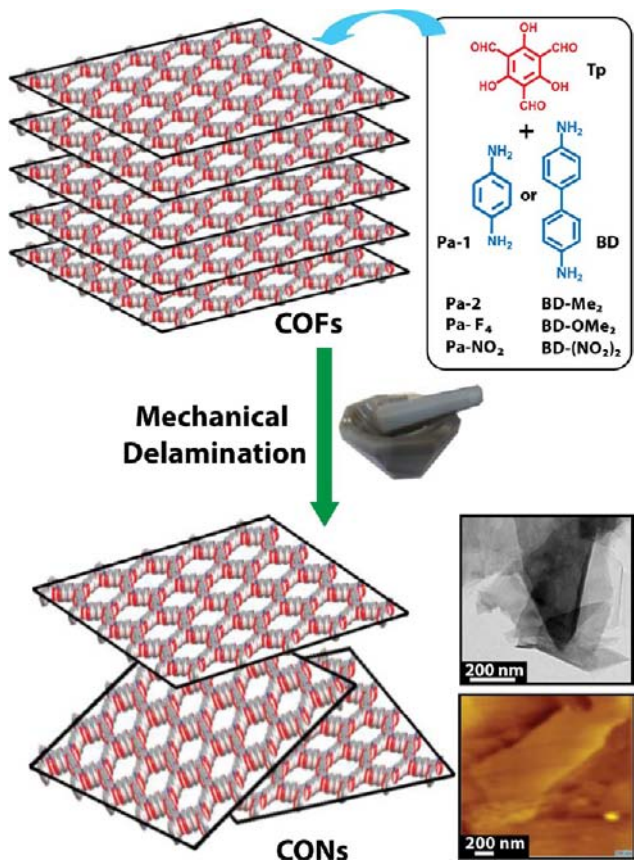
## INTRODUCTION

Covalent organic frameworks (COFs) are lightweight, crystalline porous materials ingeniously formed by strong covalent linkages between C, Si, B, N, and O.<sup>1</sup> These materials contain well-defined, predictable two-dimensional (2D) or three-dimensional (3D) ordered porous architectures and follow reticular chemistry<sup>2</sup> protocols similar to that of metal-organic frameworks (MOFs).<sup>3</sup> COFs are well known for various potential applications such as gas storage,<sup>4</sup> catalysis,<sup>5</sup> sensing,<sup>6a</sup> and optoelectronics.<sup>6a,b</sup> The majority of COFs have been synthesized utilizing selected reversible organic reactions.<sup>7</sup> Reversibility in bond formation during COF synthesis is the most essential condition for achieving good crystallinity. However, the possibility of reversible reactions makes these crystalline COFs prone to hydrolysis and subsequently hampers their sustainability even at ambient humidity. In order to address this stability issue in COFs, we have developed a synthetic protocol using combined reversible and irreversible Schiff base reactions<sup>8a,b</sup> and synthesized three stable 2D COFs (TpPa-1, TpPa-2, and TpBD), where the concept of proton tautomerism has given exceptional stability to the framework

toward water, acid, and base. Moreover, we could synthesize these COFs via an alternative solvent-free and rapid mechanochemical grinding method to substitute harsh experimental conditions (e.g., reaction in a sealed pyrex tube at high temperature and inert atmosphere) required to synthesize COFs with decent crystallinity. Interestingly, we observed some extent of delamination of the 2D COF layers during this mechanochemical synthesis, although the extent of delamination was very poor.<sup>8b</sup> Inspired by these observations, we altered our strategy and applied mechanical grinding to as-synthesized chemically stable COFs (TpPa-1, TpPa-2, and TpBD) to produce thin covalent organic nanosheets (CONs; we have used the name CONs to distinguish the materials from as-synthesized COFs) with high chemical stability. We could further extend this strategy to synthesize CONs from a library of eight crystalline, porous, functionalized COFs, namely, TpPa-1, TpPa-2, TpPa-NO<sub>2</sub>, TpPa-F<sub>4</sub>, TpBD, TpBD-(NO<sub>2</sub>)<sub>2</sub>, TpBD-Me<sub>2</sub>, and TpBD-(OMe)<sub>2</sub> (Scheme 1).

Received: August 6, 2013

Published: October 29, 2013

Scheme 1. Schematic Representation of the Formation of CONs from As-synthesized COFs via Mechanical Grinding<sup>a</sup>

<sup>a</sup>TEM and AFM images of CONs (sheetlike morphology at right bottom).

Two-dimensional materials with graphene-like features have recently attracted enormous interest due to their wide applicability toward efficient energy storage and charge transport properties.<sup>9</sup> Although there are few reports on 2D COF sheets grown on surfaces<sup>9a</sup> or synthesized by ultrasonication,<sup>10a–c</sup> these processes are highly energy consuming and need special precautions, such as the usage of dry solvents, ultrahigh vacuum, and expensive supports. Hence, a strategy to synthesize CONs by employing a simple, safe, eco-friendly, and energy efficient process is highly desirable.<sup>11,12</sup> Although this delamination method using mechanical grinding has already been utilized to synthesize graphene from graphite,<sup>10d</sup> not a single effort has been made to delaminate these chemically stable COFs using mechanical grinding. A possible reason could be the instability of most COF materials under ambient conditions, which forbids the use of mechanical force.<sup>11b</sup>

Hence, we decided to apply mechanical grinding on as-synthesized stable bulk COFs in order to extensively produce CONs. These CONs retain their structural integrity throughout the delamination process and also remain stable in aqueous, acidic, and basic media like the COF precursors.

## EXPERIMENTAL SECTION

**Synthesis of TpPa-1, TpPa-2, TpPa-NO<sub>2</sub>, TpPa-F<sub>4</sub>, TpBD, TpBD-(NO<sub>2</sub>)<sub>2</sub>, TpBD-Me<sub>2</sub>, and TpBD-(OMe)<sub>2</sub>.** The detailed synthetic procedure for TpPa-1, TpPa-2, and TpBD was described in our recent publications.<sup>8</sup> In a typical synthesis, a pyrex tube (o.d. × i.d. = 10 × 8 mm<sup>2</sup> and length = 18 cm) is charged with 0.3 mmol of

1,3,5-triformylphloroglucinol (Tp), 0.45 mmol of the corresponding diamine (2-nitro-1,4-phenylenediamine (Pa-NO<sub>2</sub>), 2,3,5,6-tetrafluoro-1,4-phenylenediamine (Pa-F<sub>4</sub>), 3,3'-dinitrobenzidine (BD-(NO<sub>2</sub>)<sub>2</sub>), *o*-tolidine (BD-Me<sub>2</sub>), and *o*-dianisidine (BD-(OMe)<sub>2</sub>)), 1.5 mL of mesitylene, 1.5 mL of 1,4-dioxane, and 0.5 mL of 3 M aqueous acetic acid (Figure 1 and Section S-2, Supporting Information). This mixture was sonicated for 10 min in order to get a homogeneous dispersion. The tube was then flash frozen at 77 K (liquid N<sub>2</sub> bath) and degassed by three freeze–pump–thaw cycles. The tube was sealed off and then heated at 120 °C for 3 days. A dark red (few COFs are yellow) colored precipitate was collected by centrifugation or filtration and washed with acetone/THF/DCM three times. The powder collected was then solvent exchanged with acetone five to six times and dried at 180 °C under vacuum for 12 h to get the corresponding COFs in ~80% isolated yield.

**Synthesis of CONs from COFs by the Mechanical Grinding Approach.** A 50 mg amount of as-synthesized COF was placed in a mortar (i.d. = 3 in. or 75 mm) and with 1–2 drops of methanol ground using a pestle at room temperature for 30 min. The dark red fine powder collected after 30 min of grinding was then dispersed in 100 mL of methanol; the resulting suspension was centrifuged at 8000 rpm for 5 min, obtaining a clear solution. The concentration of the material transferred from the settled solids to the solution as a result of mechanical grinding was calculated as 0.04 mg mL<sup>-1</sup> (~8 wt %) from the dry residue obtained after the complete evaporation of solvent as CONs. The dry powdered samples of CONs were used as such for characterization with powder X-ray diffraction (PXRD), thermogravimetric analysis (TGA), Fourier transform IR (FT-IR) spectroscopy, and so forth in order to ensure their structural stability after grinding. For transmission electron microscopy (TEM) and atomic force microscopy (AFM) imaging, we used 1 mg of CONs in 10 mL of isopropanol, sonicated for 5 min and subsequently coated on the carbon-coated copper grid (TEM) and Si-wafer or mica (AFM), and dried at room temperature prior to imaging. Similar experiments of COF delamination were also performed in a ball mill (Restch MM 400) operating at 25 Hz for 30 min, which also produces the same CONs in high isolated yield.

## RESULTS AND DISCUSSION

As revealed from PXRD analysis, COFs belonging to the TpPa series (TpPa-1, -2, -NO<sub>2</sub>, and -F<sub>4</sub>) show high crystallinity, exhibiting the first intense peak at a low angle ~4.7° (2θ), which corresponds to the (100) reflection plane, along with minor peaks at ~8.1°, ~11.1°, and ~27° (2θ), attributed to the (200), (210), and (001) reflection planes, respectively (Figure 2). Similarly, for the COFs belonging to the TpBD series (TpBD, -Me<sub>2</sub>, -(OMe)<sub>2</sub>, and -(NO<sub>2</sub>)<sub>2</sub>), the first and most intense peak corresponding to the (100) reflection plane appears at ~3.3° (2θ), with other minor peaks at ~6.3°, ~11.7°, and ~25° (2θ), attributed to the (200), (210), and (001) reflection planes, respectively. The shift of the reflection (2θ) toward the lower value of 3.3° from 4.7° for COFs belonging to the TpBD series compared to the TpPa series COFs is due to the isoreticulation, which results in larger pore aperture. The center-to-center pore distance varies from ~1.5 to ~2.4 nm, and the 2D sheets are stacked by a distance of ~3.5 Å (Figure 1). Peaks at higher 2θ correspond to the π–π stacking between the COF layers and could be assigned to the 001 reflection planes (Figure 2). In order to elucidate the structure of these COFs and to calculate the unit cell parameters, a possible 2D model was built with eclipsed and staggered stacking using the Self-Consistent Charge Density Functional Tight-Binding (SCC-DFTB) method.<sup>13a</sup> The experimental PXRD pattern matches well with the simulated pattern of the eclipsed stacking model (Figures S1, S3, S5, S7, and S9, Supporting Information). The models proposed for

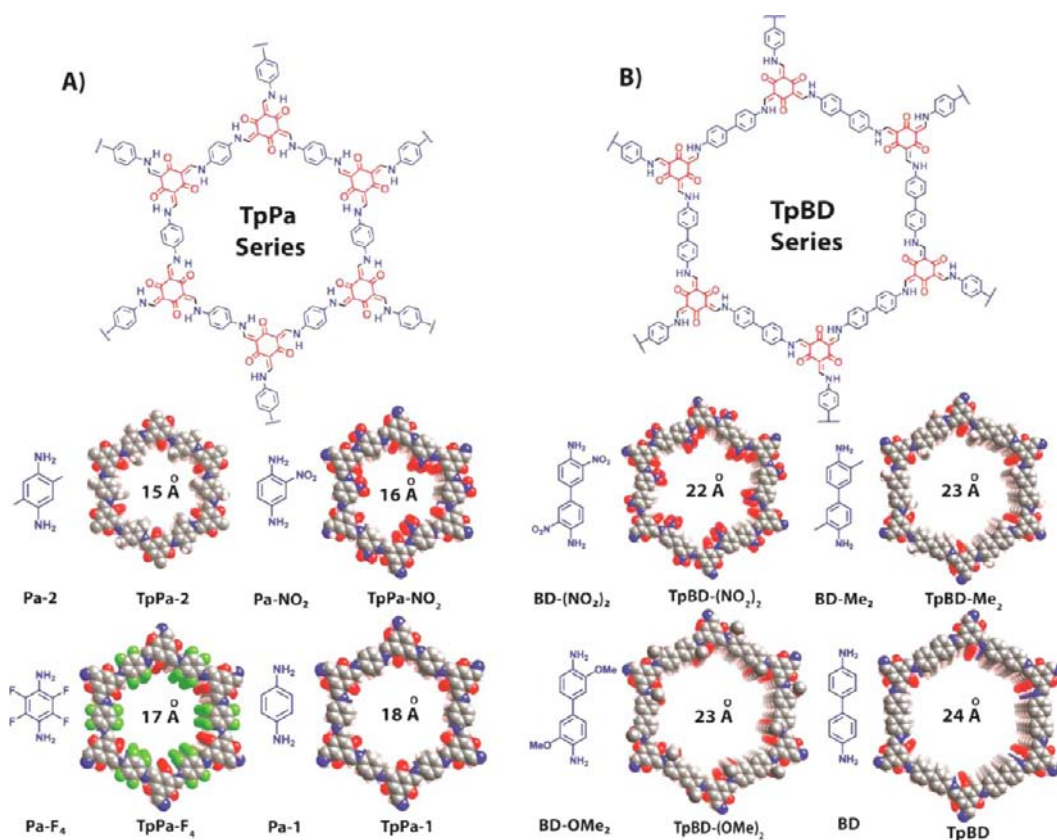


**Figure 1.** (A) TpPa series and (B) TpBD series COFs with the diamine linkers and models showing pore apertures (ascending order) of corresponding TpPa series (15–18 Å) and TpBD series (22–24 Å).

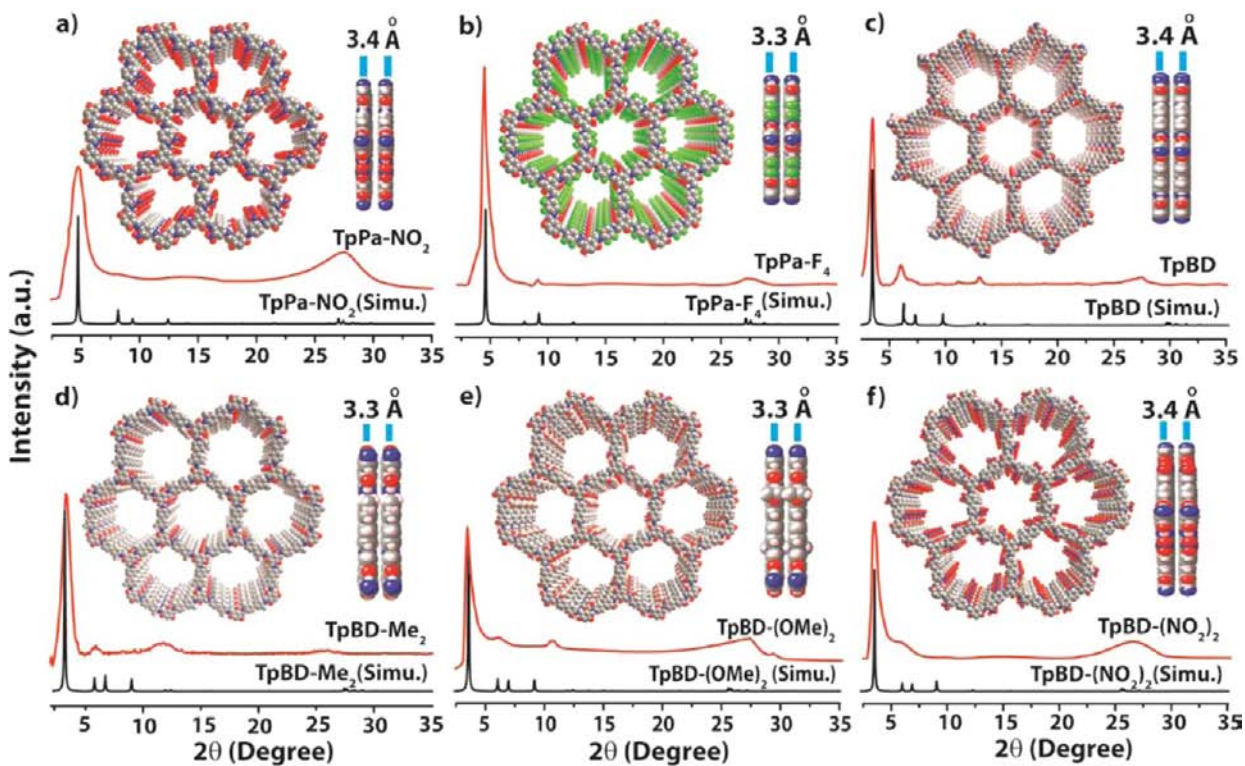


**Figure 2.** (a–f) Comparison of the PXRD patterns, red (synthesized via the solvothermal method) and black (simulated) for TpPa-NO<sub>2</sub>, TpPa-F<sub>4</sub>, TpBD, TpBD-Me<sub>2</sub>, TpBD-(OMe)<sub>2</sub>, and TpBD-(NO<sub>2</sub>)<sub>2</sub>, respectively. (Inset images showing the pore opening and π-π stacking distance between consecutive 2D layers for all COFs.)

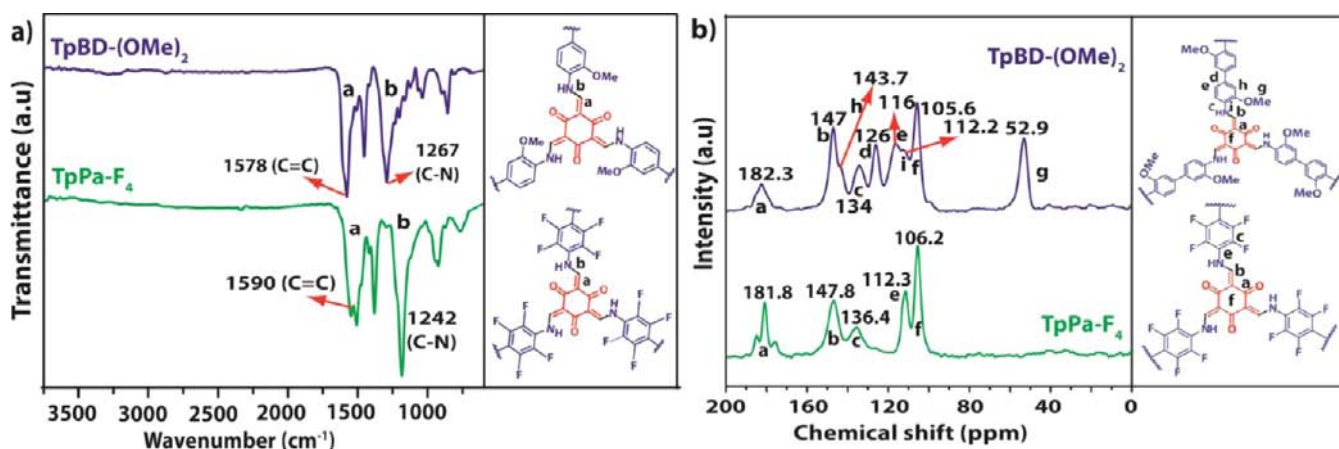


**Figure 3.** Representative (a) FT-IR spectra and (b)  $^{13}\text{C}$  CP-MAS solid-state NMR spectra of TpPa-F<sub>4</sub> and TpBD-(OMe)<sub>2</sub>. (The FT-IR and  $^{13}\text{C}$  CP-MAS solid-state NMR spectra for other COFs are provided in the Supporting Information.)

both the TpPa and TpBD series COFs are in hexagonal space group ( $P6/m$ ) except TpPa-NO<sub>2</sub>, which crystallized in the  $P1$  space group. In order to find out the unit cell parameters, Pawley refinements were done for all the COFs (Section S-3, Supporting Information). The proposed 2D models and the detailed structural description of TpPa-1 ( $a = b = 22.1 \text{ \AA}$ ,  $c = 3.3 \text{ \AA}$ ), TpPa-2 ( $a = b = 22.1 \text{ \AA}$ ,  $c = 3.3 \text{ \AA}$ ), and TpBD ( $a = b = 30.48594 \pm 0.18236 \text{ \AA}$ ,  $c = 3.39756 \pm 0.02065 \text{ \AA}$ ) were presented in our previous publications.<sup>8</sup> However, the unit cell parameters for other COFs such as TpPa-NO<sub>2</sub> were found to be  $a = 21.83899 \pm 1.63753 \text{ \AA}$ ,  $b = 21.83899 \pm 1.63753 \text{ \AA}$ , and  $c = 3.24413 \pm 0.24504 \text{ \AA}$ , and for TpPa-F<sub>4</sub>, the values obtained were  $a = b = 20.90054 \pm 3.20024 \text{ \AA}$  and  $c = 3.49949 \pm 0.500764 \text{ \AA}$ . Similarly, the unit cell parameters have been obtained for TpBD-(NO<sub>2</sub>)<sub>2</sub> ( $a = b = 43.97281 \pm 0.90651 \text{ \AA}$ ,  $c = 3.70926 \pm 0.40028 \text{ \AA}$ ), TpBD-Me<sub>2</sub> ( $a = b = 33.61975 \pm 2.35616 \text{ \AA}$ ,  $c = 3.03143 \pm 0.21548 \text{ \AA}$ ), and TpBD-(OMe)<sub>2</sub> ( $a = b = 28.77893 \pm 0.02801 \text{ \AA}$ ,  $c = 3.25 \pm 0.0000 \text{ \AA}$ ) (Section S-3, Table S-6, Supporting Information). It was reported in the literature that, in 2D COFs, parallel displaced structures have got more preference over the fully eclipsed AA stacking.<sup>13b-d</sup> To prove this, we had done the modeling of the parallel displaced structures of the functionalized COFs (TpPa-NO<sub>2</sub>, TpPa-F<sub>4</sub>, TpBD-(NO<sub>2</sub>)<sub>2</sub>, TpBD-Me<sub>2</sub>, and TpBD-(OMe)<sub>2</sub>). The energy calculation shows that the parallel displaced structure is more stable than the fully eclipsed AA stacking, even though, there was no difference in the simulated PXRD pattern (Section S-3A, Table S7, Supporting Information). The lack of high crystallinity forces us to adopt a static model rather than a dynamic disordered model for all these COFs. However, one must acknowledge that there is a very high possibility for these COFs to adopt a disordered structure.

The FT-IR spectra obtained for all these COFs clearly indicate the complete disappearance of IR bands corresponding to the characteristic N-H stretching ( $3100\text{--}3300 \text{ cm}^{-1}$ ) of the free diamine (Pa-1, Pa-2, Pa-NO<sub>2</sub>, Pa-F<sub>4</sub>, BD, BD-(NO<sub>2</sub>)<sub>2</sub>, BD-Me<sub>2</sub>, and BD-(OMe)<sub>2</sub>) and the carbonyl stretching band ( $1639 \text{ cm}^{-1}$ ) of 1,3,5-triformylphloroglucinol (Tp) (Figure 3a and Section S-4, Supporting Information). Interestingly, the FT-IR spectrum of any COF reported in this paper does not show the characteristic stretching bands of hydroxyl (-OH) or imine (C=N) functional groups, which should have been present if the compound existed in the enol form. Instead, it shows a strong peak at  $\sim 1582 \text{ cm}^{-1}$  for both the TpPa series (TpPa-1,

-2, -NO<sub>2</sub>, and -F<sub>4</sub>) and the TpBD series (TpBD, -(NO<sub>2</sub>)<sub>2</sub>, -Me<sub>2</sub>, and -(OMe)<sub>2</sub>), which arises due to the C=C stretching band. This C=C stretching band at  $1582 \text{ cm}^{-1}$  appears due to the enol to keto tautomerism, which has been observed in the FT-IR spectrum of the reference compound 2,4,6-tris[(phenylamino)methylene] cyclohexane-1,3,5-trione<sup>14</sup> (Figure S11, Supporting Information). All eight COFs reported in this paper showed similar FT-IR spectra. The little variation in the peak positions that is observed arises due to the different functional groups present at the diamine linkers. In some cases, the peak broadening was observed in the extended structures, when C=O peaks ( $\sim 1616 \text{ cm}^{-1}$ ) get merged with C=C stretching bands ( $\sim 1582 \text{ cm}^{-1}$ ) and appear as shoulders. This confirms the overall s-cis structure in each COF presented in this study. The appearance of two peaks at  $\sim 1445$  and  $\sim 1256 \text{ cm}^{-1}$  correspond to the aromatic C=C and newly formed C-N bond in the keto form of all COFs. The FT-IR spectrum of TpPa-2 and TpBD-Me<sub>2</sub> shows an extra peak at  $\sim 2885 \text{ cm}^{-1}$ , which is due to the C-H stretching from the methyl (-CH<sub>3</sub>) functionality. Similarly, for TpPa-NO<sub>2</sub> and TpBD-(NO<sub>2</sub>)<sub>2</sub>, a peak appears exactly at  $1506 \text{ cm}^{-1}$ , which corresponds to the -NO<sub>2</sub> functionality and confirms its presence in the framework.

We carried out  $^{13}\text{C}$  CP-MAS solid-state NMR spectroscopy to verify the atomic-level construction of COFs presented in this paper. The individual spectrum obtained was compared with other members of the same series (Figure 3b and Section S-5, Supporting Information). The solid-state NMR of the reference compound 2,4,6-tris[(phenylamino)methylene] has also been presented in Figure S19 of the Supporting Information for comparison. All COFs reported in this paper showed a signal at  $\sim 180\text{--}182 \text{ ppm}$ , which could be ascribed as the carbonyl carbon [C=O] of the keto form. The peak at  $\sim 144 \text{ ppm}$  confirms the presence of the C-N bond, instead of the C=N bond ( $\sim 165 \text{ ppm}$ ), which could have been a signature peak if these COFs would have existed in the enol form. The unobserved peak at  $\sim 190 \text{ ppm}$  (for -CHO) gives clear evidence for the complete consumption of the starting material (Tp). The appearance of a peak at  $\sim 124 \text{ ppm}$  is due to the carbons present at the biphenyl junction of benzidine (BD) in the TpBD series. Such a peak is also present in the  $^{13}\text{C}$  spectra of TpPa-2 and TpPa-NO<sub>2</sub> due to unsymmetrical substitution and absent in TpPa-1 and TpPa-F<sub>4</sub> COFs due to the symmetrical substitution at 2,3,5,6 positions of the aromatic

diamines (Pa-1 and Pa-F<sub>4</sub>). In the case of TpPa-2 and TpBD-Me<sub>2</sub>, there is a <sup>13</sup>C NMR peak exactly at 14 ppm that arises due to the presence of an extra methyl (–CH<sub>3</sub>) functionality, unlike the other COFs (Figure S19, Supporting Information). However, for TpBD-(OMe)<sub>2</sub>, the methyl carbon peak (52.9 ppm) gets deshielded as it is attached to the oxygen of the methoxy (–OMe) functionality.

External morphologies of these as-synthesized COFs were investigated by employing SEM and TEM imaging that showed COFs belonging to the TpPa and TpBD series crystallize with a flowerlike morphology (Section S-8, Supporting Information). Each individual flower can be considered as a result of aggregation of a large number of petals that have length in the micrometer range (1–3 μm). In the case of the TpPa series COFs, petals (70–150 nm width and 30–40 nm thickness) have spike-shaped tips and have grown out from a core, whereas for the TpBD series COFs, petals are grown with a broader width to form platelike structures (1–5 μm length, 100–200 width, and 50–70 nm thickness). We would assume that individual petals have sheetlike structures (Figure 6) and can be formed as a result of π–π stacking of different COF layers. In order to check the thermal stability of all eight COFs, we have performed TGA under a flow of N<sub>2</sub> gas. It has been observed from the TGA profiles that all COF pores are guest free and have almost identical thermal stabilities up to ~350 °C (Section S-7, Supporting Information) except for TpPa-NO<sub>2</sub> and TpBD-(NO<sub>2</sub>)<sub>2</sub>, where the framework is stable up to 300 °C. After 350 °C, these COFs start decomposing with gradual weight loss between 45–60% for all COFs until 800 °C.

N<sub>2</sub> adsorption isotherms at 77 K were performed to examine the architectural rigidity and permanent porosity of all aforementioned COFs. All COFs showed typical type I reversible isotherms (Figure 4a,b). The Brunauer–Emmett–

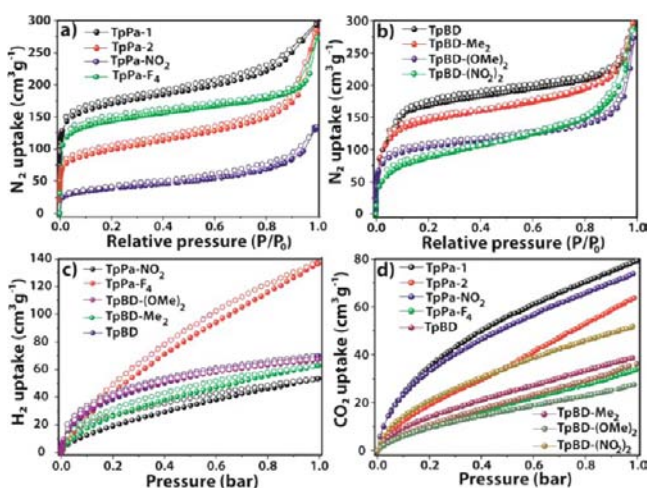


**Figure 4.** (a,b) Comparison of N<sub>2</sub> adsorption isotherms of TpPa series and TpBD series, respectively; (c) H<sub>2</sub> sorption isotherms of TpPa-NO<sub>2</sub>, TpPa-F<sub>4</sub>, TpBD-(OMe)<sub>2</sub>, TpBD-Me<sub>2</sub>, and TpBD at 77 K; (d) CO<sub>2</sub> uptake of all eight COFs at 273 K. (Filled spheres for adsorption and hallow spheres for desorption.)

Teller (BET) surface area for the activated TpBD was found to be 537 m<sup>2</sup> g<sup>-1</sup>, which is the highest among the TpBD series COFs, whereas for other COFs of this series, the values are 468 m<sup>2</sup> g<sup>-1</sup> (TpBD-Me<sub>2</sub>), 330 m<sup>2</sup> g<sup>-1</sup> (TpBD-(OMe)<sub>2</sub>), and 295 m<sup>2</sup> g<sup>-1</sup> (TpBD-(NO<sub>2</sub>)<sub>2</sub>). TpPa-1 possesses the highest BET surface area value of 535 m<sup>2</sup> g<sup>-1</sup>, higher than the other COFs

of the TpPa series such as TpPa-F<sub>4</sub> (438 m<sup>2</sup> g<sup>-1</sup>), TpPa-2 (339 m<sup>2</sup> g<sup>-1</sup>), and TpPa-NO<sub>2</sub> (129 m<sup>2</sup> g<sup>-1</sup>). The lower surface area values for the keto-enamine based COFs are probably due to the lower reversibility in the COF formation reaction. The incorporation of a bulky functional group on the COF pore wall decreases the surface area in the case of TpPa-NO<sub>2</sub> and TpPa-F<sub>4</sub> due to the blocking of the COF pore walls. The introduction of a functional group at the 3, 3' position in the biphenyl ring system disturbs the planarity of the diamine ligands that can be the reason for the low crystallinity and surface area of the functionalized TpBD COF series. The pore size distributions for all COFs (both TpPa and TpBD series) have been presented in the Supporting Information and were found to be between 1.0 and 1.7 nm, calculated on the basis of nonlocal density functional theory (NLDFT) (Figure S22-A, Supporting Information). It is well known that polar functional groups present in porous materials such as MOFs and COFs have impact on H<sub>2</sub> uptake. Since these COFs contain a variety of functional groups decorated throughout the framework, we decided to perform H<sub>2</sub> and CO<sub>2</sub> adsorption experiments at 77 and 273 K, respectively. The H<sub>2</sub> uptake capacity of TpPa-F<sub>4</sub> was found to be the highest (136 cm<sup>3</sup> g<sup>-1</sup>) among all the COFs presented in this paper, such as TpPa-1 (110 cm<sup>3</sup> g<sup>-1</sup>), TpPa-2 (89 cm<sup>3</sup> g<sup>-1</sup>), TpBD (69 cm<sup>3</sup> g<sup>-1</sup>), TpPa-NO<sub>2</sub> (53 cm<sup>3</sup> g<sup>-1</sup>), TpBD-Me<sub>2</sub> (62 cm<sup>3</sup> g<sup>-1</sup>), TpBD-(OMe)<sub>2</sub> (67 cm<sup>3</sup> g<sup>-1</sup>), and TpBD-(NO<sub>2</sub>)<sub>2</sub> (40 cm<sup>3</sup> g<sup>-1</sup>) (Figure 4c and Figure S23, Supporting Information). The polar interactions of the C–F bond with the H<sub>2</sub> gas molecules could be the reason for high H<sub>2</sub> uptake in TpPa-F<sub>4</sub>. Interestingly, the CO<sub>2</sub> uptake of TpPa-1 (80 cm<sup>3</sup> g<sup>-1</sup> at 273 K) is the highest among all COFs presented in this work, such as TpPa-NO<sub>2</sub> (73 cm<sup>3</sup> g<sup>-1</sup>), TpPa-2 (63 cm<sup>3</sup> g<sup>-1</sup>), TpBD-(NO<sub>2</sub>)<sub>2</sub> (52 cm<sup>3</sup> g<sup>-1</sup>), TpBD (40 cm<sup>3</sup> g<sup>-1</sup>), TpBD-Me<sub>2</sub> (37 cm<sup>3</sup> g<sup>-1</sup>), TpPa-F<sub>4</sub> (35 cm<sup>3</sup> g<sup>-1</sup>), and TpBD-(OMe)<sub>2</sub> (27 cm<sup>3</sup> g<sup>-1</sup>) (Figure 4d). We have also collected the water vapor adsorption isotherms for all COFs and found that TpBD possesses the highest water vapor uptake of 265 cm<sup>3</sup> g<sup>-1</sup> at 0.9 (P/P<sub>0</sub>) and 20 °C (at STP), closely followed by TpBD-Me<sub>2</sub> (255 cm<sup>3</sup> g<sup>-1</sup>), TpBD-(OMe)<sub>2</sub> (250 cm<sup>3</sup> g<sup>-1</sup>), and TpPa-NO<sub>2</sub> (223 cm<sup>3</sup> g<sup>-1</sup>) (Section S-6, Figure S24, Supporting Information).

To investigate the chemical stability of these COFs in water, we have submerged 50 mg of COF materials in 10 mL of deionized water and allowed it to stand for 7 days under boiling condition (100 °C). After the mentioned period, we took the PXRD to confirm the crystallinity and found that all PXRD peak positions as well as the intensity retained after 7 days, which indicates the stability of these COFs in boiling water for a period of 7 days or beyond (Figure 5). This water stability arises due to the irreversible nature of the enol-to-keto tautomerism, where the equilibrium is driven by the relative base strength of the imine nitrogen (C=N) over the phenolic oxygen (O–H) existing in the tris(*N*-salicylideneanilines) moiety. Previously, it has been observed that TpPa-1 and TpPa-2 were quite stable in acid (9 N HCl) up to a period of 7 days. Similarly, other COFs of both the TpPa and TpBD series are also stable in acid (3–9 N HCl) and in base. This has been confirmed by the identical peak positions and intensities in the PXRD profile collected after the acid treatment for 3–7 days. It is to be noted that TpBD and TpBD-(NO<sub>2</sub>)<sub>2</sub> are stable up to 7 days in 9 N HCl like TpPa-1 and TpPa-2, whereas the rest of the COFs are stable up to 3 days (Figure 5). The characteristic IR peaks of as-synthesized COFs do match very well with the acid-treated COFs (Figure S33, Supporting Information). In

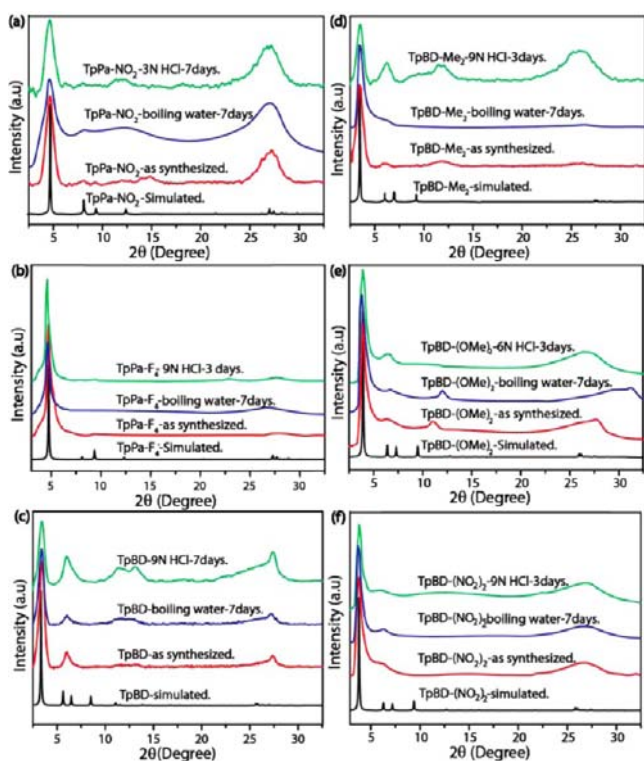


**Figure 5.** (a–f) PXRD patterns showing water and acid stability for TpPa-NO<sub>2</sub>, TpPa-F<sub>4</sub>, TpBD, TpBD-Me<sub>2</sub>, TpBD-(OMe)<sub>2</sub>, and TpBD-(NO<sub>2</sub>)<sub>2</sub>, respectively, after dipping 1 week in boiling water and in 3–9 N HCl.

terms of base stability, TpPa-2, TpBD, TpBD-Me<sub>2</sub>, and TpBD-(OMe)<sub>2</sub> are stable in 3 N NaOH for 3 days whereas TpPa-1, TpPa-NO<sub>2</sub>, TpPa-F<sub>4</sub>, and TpBD-(NO<sub>2</sub>)<sub>2</sub> are not stable in base for even a day (Section S-11, Figure S34, Supporting Information).

Since the synthesis of 2D organic nanomaterials is currently of emerging interest in the field of nanoscience,<sup>15</sup> one would assume that CONs, synthesized via delamination of 2D COF layers, could be a potential 2D organic nanomaterial. It is noteworthy that there have only been a few reports on the delamination of as-synthesized COFs, where bulk layered COFs have been exfoliated into thin flat nanostructures by ultrasonication.<sup>10a–c</sup> This delamination of COFs via ultrasonication requires ultrapure and absolutely dry solvents. On the other hand, 2D COFs have also been grown on expensive graphite (e.g., HOPG), single-layer graphene (SLG), or Ag supports using ultrahigh vacuum.<sup>9a</sup> Such precautions required for the delamination is mainly due to the instability of COFs under ambient conditions. Hence, in order to delaminate COFs in a more efficient manner, we used the mechanical grinding approach and applied this approach to all eight as-synthesized COFs (both TpPa and TpBD series) reported here. We anticipated that mechanical grinding will facilitate the separation of existing  $\pi$ – $\pi$  staking (AA) between the stable COFs layers. All these COFs have many similarities to graphite with respect to dimensionality, periodic, parallel lattices, and almost identical stacking distance between consecutive layers ( $\sim$ 3.4–3.6 Å). Like graphite, due to the presence of strong in-plane bonds and weak van der Waals interactions between layers in COFs, there is sufficient opportunity to delaminate such materials into individual layers either by chemical or mechanical delamination. This mechanical delamination

approach was found to be more effective over ultrasonication or layer growth as it does not require ultrapure and dry solvents or expensive supports. In order to test the existence of nanosheet-like structures, well-dispersed mechanically grinded COFs were suspended in isopropanol. This suspension has been deposited on a carbon-coated copper grid and observed by means of TEM. Figure 6, columns 2 and 3, shows typical images observed using TEM. As a result of delamination, we observed very thin graphite-like layered structures (100 nm to 1  $\mu$ m length) from TEM images all around the grid for all grinded COFs (Figure 6, column 3, and Section S-9, Supporting Information). The laminar structure of the materials (CONs) obtained by mechanical grinding of as-synthesized COFs was assessed by AFM measurements in order to obtain precise information about the existence of single-/few-layer materials. In order to isolate a few thin layers of CONs on surfaces, the sufficiently dilute solution (see the Experimental Section) of CONs was deposited by drop-casting on mica and SiO<sub>2</sub> surfaces. These CONs show flat nanosheet-like structures with lengths and widths of several micrometers and thicknesses ranging from 3 to 10 nm, which corresponds to the existence of only  $\sim$ 10–30 COF layers (Section S-9, Supporting Information). The images obtained in some cases clearly show terraces with steps indicating distinct levels of delamination in the same nanostructures, suggesting multilayer structures. The information obtained from AFM imaging is in good agreement with the TEM images. As shown in high-resolution (HR)-TEM images, some fringes have been observed like graphite-type layered material with periodic distance of  $\sim$ 0.34 nm along one direction (Figures S30 and S31, Supporting Information). We believe that, when subjected to strong mechanical force, the 2D layers of these COFs get easily delaminated producing nanosheet-like structures. In order to further characterize these CONs, we have used FT-IR and Raman spectroscopies that showed exactly similar spectra like the as-synthesized COFs and revealed that the compositions, as well as the mode of bonding, are still intact after the mechanical grinding (Figure 6, column 4, and Section S-14, Supporting Information). Similarly, to check the crystallinity after grinding, we carried out PXRD of these CONs and observed that the PXRD profile remained the same as that of the as-synthesized samples (Figure 6, column 5). However, a decrease in intensity of the first peak (100 plane) and the broadening of the last peak (001 plane) have been observed, which is the only difference between the PXRD of the COFs and the CONs (Figure 6, column 4). This could be due to the random displacement of the 2D layers (delaminated) as the distributions of eclipsed pores get affected. As a result, the reflection corresponding to the 100 plane becomes weak. The broader peak at higher  $2\theta$  ( $\sim$ 27°) is due to the lack of  $\pi$ – $\pi$  staking between the COF layers, which is strongly affected by the reduction of the number of stacked layers in these thin CONs. TGA was performed for all CONs to get information about the thermal stability. Comparison of the TGA curves of CONs and COFs reported in this paper shows that they have almost similar decomposition profiles (Section S-7, Supporting Information).

N<sub>2</sub> adsorption experiments have also been performed for these CONs to check the effect of surface area upon mechanical grinding. The isotherms obtained are type I like as-synthesized COFs, but the surface area decreases drastically (Figures S20 and S21, Supporting Information). The exact reason for the lower surface area for these CONs is not fully clear to us, but

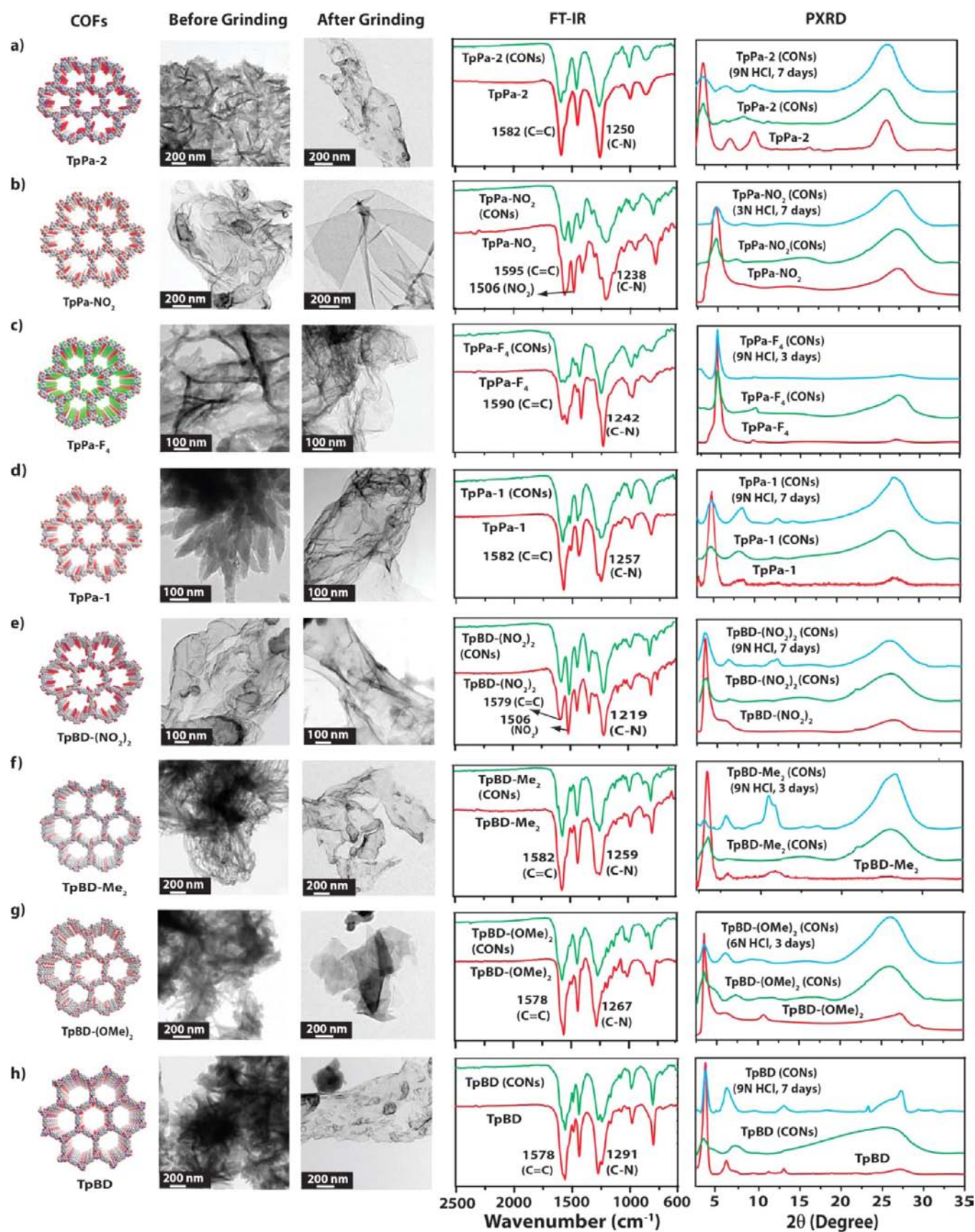


**Figure 6.** (a–h) Packing diagrams, HR-TEM images (before grinding), HR-TEM images of delaminated COFs (after grinding), FT-IR spectra of as-synthesized COFs (red) with corresponding delaminated COFs (CONs) (green), and PXRD patterns of as-synthesized COFs (red), corresponding delaminated COFs (CONs) (green), and acid-treated CONs (cyan).

we speculate that mechanical grinding can create disorder in the  $\pi$ - $\pi$  stacking, which was understood by the broad nature of the 001 peak in the PXRD pattern of CONs (Figure 6). Due to this defect in  $\pi$ - $\pi$  stacking, there is a chance of layer flipping in COFs that results in thin layered structures (Figure 6, column 3), and the long-range pore structure of the COFs gets disturbed followed by only less depth pores accessible for  $N_2$  sorption. As far as the chemical stability is concerned, it has been found that these CONs retain their structural integrity throughout the delamination process and also remain stable in aqueous, acidic (3–9 N HCl) and basic (3 N NaOH) media like the parent COFs, which is confirmed by PXRD and IR analyses (Figure 6, column 5, and Section S-12, Supporting Information). This kind of mechanical delamination by grinding has already been known for graphene and other 2D materials, but this is the first report of mechanical delamination of as-synthesized COFs to CONs. After the mechanical grinding process, we suspended some CONs material into methanol and subsequently passed green laser light (532 nm) into the solution to check the dispersive nature of the particles. Interestingly, the suspension showed Tyndall effect (Figure S38, Supporting Information), which the characteristic phenomenon is typically seen in colloidal solution under a light source, which further confirms the highly dispersive and fine particle nature of these CONs.

## CONCLUSION

In summary, we have for the first time synthesized a library of five chemically stable COFs, namely, TpPa-NO<sub>2</sub>, TpPa-F<sub>4</sub>, TpBD-(NO<sub>2</sub>)<sub>2</sub>, TpBD-Me<sub>2</sub>, and TpBD-(OMe)<sub>2</sub> along with three previously reported ones (TpPa-1, TpPa-2, and TpBD) using the simple Schiff base reaction. By adopting different functionalized diamines, we could construct these COFs with variable pore apertures ranging from 15 to 24 Å. These COFs are crystalline, porous, and exceptionally stable in aqueous, acidic, and basic media. The synthesized COFs (all eight) were successfully delaminated by using a simple, safe, and environmentally friendly mechanical grinding route, leading to their transformation into thin layered CONs. These exfoliated CONs have graphene-like layered morphology unlike parent COFs. We believe that the stability of these COF layers is the main reason for this delamination. Since these individual layers with intrinsic chemical stability are stacked on top of each other with  $\pi$ - $\pi$  stacking interactions, a mild mechanical force easily delaminates the layers from each other. As mechanical grinding is a scalable and energy efficient method compared to other existing methods such as ultrasonication, CVD, and layer growth, we believe that this “top-down” strategy will provide a cost-effective and scalable approach for the preparation of novel bulk 2D-layered materials in the near future. Also, the observed 2D-layered structures of these CONs have the potential to act as a graphene-like supportive material for a wide variety of energy or imaging applications.

## ASSOCIATED CONTENT

### Supporting Information

General information; synthetic procedures; structural modeling and PXRD analysis; FT-IR, <sup>13</sup>C solid-state NMR, and Raman spectra; gas/water adsorption studies; TGA; SEM; TEM; AFM; stability studies; Tyndall effect; and crystallographic data. This material is available free of charge via the Internet at <http://pubs.acs.org>.

## AUTHOR INFORMATION

### Corresponding Author

r.banerjee@ncl.res.in

### Notes

The authors declare no competing financial interests.

## ACKNOWLEDGMENTS

S.C. and B.P.B. acknowledge UGC, and S.K. acknowledges CSIR for JRF. R.B. acknowledges CSIR's Five Year Plan Project (CSC0122 and CSC0102) for funding. Financial assistance from BRNS (2011/37C/44/BRNS) is acknowledged. We acknowledge Dr. T. G. Ajithkumar for providing NMR and Dr. C. Ramesh for PXRD facilities.

## REFERENCES

- (1) (a) Côté, A. P.; Benin, A. I.; Ockwig, N. W.; Matzger, A. J.; O'Keeffe, M.; Yaghi, O. M. *Science* **2005**, *310*, 1166–1170. (b) Feng, X.; Ding, X.; Jiang, D. *Chem. Soc. Rev.* **2012**, *41*, 6010–6022. (c) Dienstmaier, J. F.; Medina, D. D.; Dogru, M.; Knochel, P.; Bein, T.; Heckl, W. M.; Lackinger, M. *ACS Nano* **2012**, *6*, 7234–7242. (d) Kuhn, P.; Antonietti, M.; Thomas, A. *Angew. Chem., Int. Ed.* **2008**, *47*, 3450–3453. (e) Dogru, M.; Handloser, M.; Auras, F.; Kunz, T.; Medina, D.; Hartschuh, A.; Knochel, P.; Bein, T. *Angew. Chem., Int. Ed.* **2013**, *52*, 2920–2924.
- (2) (a) Uribe-Romo, F. J.; Hunt, J. R.; Furukawa, H.; Klock, C.; O'Keeffe, M.; Yaghi, O. M. *J. Am. Chem. Soc.* **2009**, *131*, 4570–4571. (b) Wan, S.; Guo, J.; Kim, J.; Ihee, H.; Jiang, D. L. *Angew. Chem., Int. Ed.* **2008**, *47*, 8826–8830. (c) Zwaneveld, N. A. A.; Pawlak, R.; Abel, M.; Catalin, D.; Gigmes, D.; Bertin, D.; Porte, L. *J. Am. Chem. Soc.* **2008**, *130*, 6678–6679.
- (3) Deng, H.; Grunder, S.; Cordova, K. E.; Valente, C.; Furukawa, H.; Hmadeh, M.; Gándara, F.; Whalley, A. C.; Liu, Z.; Asahina, S.; Kazumori, H.; O'Keeffe, M.; Terasaki, O.; Stoddart, J. F.; Yaghi, O. M. *Science* **2012**, *336*, 1018–1023.
- (4) (a) Doonan, C. J.; Tranchemontagne, D. J.; Glover, T. G.; Hunt, J. R.; Yaghi, O. M. *Nat. Chem.* **2010**, *2*, 235–238. (b) Furukawa, H.; Yaghi, O. M. *J. Am. Chem. Soc.* **2009**, *131*, 8875–8883.
- (5) Ding, S. Y.; Gao, J.; Wang, Q.; Zhang, Y.; Song, W. G.; Su, C. Y.; Wang, W. *J. Am. Chem. Soc.* **2011**, *133*, 19816–19822.
- (6) (a) Wan, S.; Guo, J.; Kim, J.; Ihee, H.; Jiang, D. L. *Angew. Chem., Int. Ed.* **2009**, *48*, 5439–5442. (b) Anthony, J. E. *Chem. Rev.* **2006**, *106*, 5028–5048.
- (7) (a) Côté, A. P.; El-Kaderi, H. M.; Furukawa, H.; Hunt, J. R.; Yaghi, O. M. *J. Am. Chem. Soc.* **2007**, *129*, 12914–12915. (b) Wan, S.; Guo, J.; Kim, J.; Ihee, H.; Jiang, D. *Angew. Chem., Int. Ed.* **2008**, *120*, 8958–8962.
- (8) (a) Kandambeth, S.; Mallick, A.; Lukose, B.; Mane, V. M.; Heine, T.; Banerjee, R. *J. Am. Chem. Soc.* **2012**, *134*, 19524–19527. (b) Biswal, B. P.; Chandra, S.; Kandambeth, S.; Lukose, B.; Mane, V. M.; Heine, T.; Banerjee, R. *J. Am. Chem. Soc.* **2013**, *135*, 5328–5331.
- (9) (a) Colson, J. W.; Woll, A. R.; Mukherjee, A.; Levendorf, M. P.; Spitler, E. L.; Shields, V. B.; Spencer, M. G.; Park, J.; Dichtel, W. R. *Science* **2011**, *332*, 228–231. (b) Coropceanu, V.; Cornil, J.; da Silva Filho, D. A.; Olivier, Y.; Silbey, R.; Bredas, J.-L. *Chem. Rev.* **2007**, *107*, 926–952. (c) Marele, A. C.; Mas-Balleste, R.; Terracciano, L.; Rodriguez-Fernandez, J.; Berlanga, I.; Alexandre, S. S.; Otero, R.; Gallego, J. M.; Zamora, F.; Gomez-Rodriguez, J. M. *Chem. Commun.* **2012**, *48* (6), 779–6781. (d) Abel, M.; Clair, S.; Ourdjini, O.; Mossayan, M.; Porte, L. *J. Am. Chem. Soc.* **2011**, *133*, 1203–1205. (e) Liu, X. H.; Guan, C.-Z.; Ding, S.-Y.; Wang, W.; Yan, H.-J.; Wang, D.; Wan, L.-J. *J. Am. Chem. Soc.* **2013**, *135*, 10470–10474.
- (10) (a) Berlanga, I.; Ruiz-Gonzalez, M. L.; Gonzalez-Calbet, J. M.; Fierro, J. L. G.; Mas-Balleste, R.; Zamora, F. *Small* **2011**, *7*, 1207–1211. (b) Berlanga, I.; Mas-Balleste, R.; Zamora, F. *Chem. Commun.* **2012**, *48*, 7976–7978. (c) Bunck, D. N.; Dichtel, W. R. *J. Am. Chem. Soc.* **2013**, *135* (40), 14952–14955. (d) Jeon, I.-Y.; Choi, H.-J.; Jung,

S.-M.; Seo, J.-M.; Kim, M.-J.; Dai, L.; Baek, J.-B. *J. Am. Chem. Soc.* **2013**, *135*, 1386–1393.

(11) (a) Friščić, T. *Chem. Soc. Rev.* **2012**, *41*, 3493–3510. (b) Lanni, L. M.; Tilford, R. W.; Bharathy, M.; Lavigne, J. J. *J. Am. Chem. Soc.* **2011**, *130*, 13975–13983. (c) Stojakovic, J.; Farris, B. S.; MacGillivray, L. R. *Chem. Commun.* **2012**, *48*, 7958–7960. (d) Braga, D.; Grepioni, F. *Angew. Chem., Int. Ed.* **2004**, *43*, 4002–4011. (e) Friščić, T.; Halasz, I.; Beldon, P. J.; Belenguer, A. M.; Adams, F.; Kimber, S. A. J.; Honkimäki, V.; Dinnebier, R. E. *Nat. Chem.* **2013**, *5*, 66–73. (f) James, S. L.; Adams, C. J.; Bolm, C.; Braga, D.; Collier, P.; Friscic, T.; Grepioni, F.; Harris, K. D. M.; Hyett, G.; Jones, W.; Krebs, A.; Mack, J.; Maini, L.; Orpen, A. G.; Parkin, I. P.; Shearouse, W. C.; Steed, J. W.; Waddell, D. C. *Chem. Soc. Rev.* **2012**, *41*, 413–447.

(12) Tan, J. C.; Saines, P. J.; Bithell, E. G.; Cheetham, A. K. *ACS Nano* **2012**, *6*, 615–621.

(13) (a) Heine, T.; Rapacioli, M.; Patchkovskii, S.; Frenzel, J.; Koester, A. M.; Calaminici, P.; Escalante, S.; Duarte, H. A.; Flores, R.; Geudtner, G.; Goursot, A.; Reveles, J. U.; Vela, A.; Salahub, D. R. *deMon-nano*; Jacobs University Bremen: Bremen, Germany, 2009. (b) Lukose, B.; Kuc, A.; Heine, T. *Chem.—Eur. J.* **2011**, *17*, 2388–2392. (c) Ding, X.; Chen, L.; Honsho, Y.; Feng, X.; Saengsawang, O.; Guo, J.; Saeki, A.; Seki, S.; Irle, S.; Nagase, S.; Parasuk, V.; Jiang, D. *J. Am. Chem. Soc.* **2011**, *133*, 14510–14513. (d) Jin, S.; Furukawa, K.; Addicoat, M.; Chen, L.; Takahashi, S.; Irle, S.; Nakamura, T.; Jiang, D. *Chem. Sci.* **2013**, *4*, 4505–4511.

(14) Chong, J. H.; Sauer, M.; Patrick, B. O.; MacLachlan, M. *Org. Lett.* **2003**, *5*, 3823–3826.

(15) (a) Blunt, M. O.; Russell, J. C.; Giménez-López, M. C.; Lin, X.; Garrahan, J. P.; Schröder, M.; Champness, N. R.; Beton, P. H. *Science* **2008**, *322*, 1077–1081. (b) Ahn, S.; Morrison, C. N.; Matzger, A. J. *J. Am. Chem. Soc.* **2009**, *131*, 7946–7947. (c) Ballesté, R. M.; Navarro, C. G.; Herrero, J. G.; Zamora, F. *Nanoscale* **2011**, *3*, 20–30. (d) Yan, L.; Zheng, Y. B.; Zhao, F.; Li, S.; Gao, X.; Xu, B.; Weiss, P. S.; Zhao, Y. *Chem. Soc. Rev.* **2012**, *41*, 97–114. (e) Ciesielski, A.; Szabelski, P. J.; Rzyzko, W.; Cadeddu, A.; Cook, T. R.; Stang, P. J.; Samorì, P. *J. Am. Chem. Soc.* **2013**, *135*, 6942–6950. (f) Sainsbury, T.; Satti, A.; May, P.; O'Neill, A.; Nicolosi, V.; Gun'ko, Y. K.; Coleman, J. N. *Chem.—Eur. J.* **2012**, *18*, 10808–10812. (g) Liu, W. W.; Wang, J. N. *Chem. Commun.* **2011**, *47*, 6888–6890. (h) Wang, X. Q.; Fulvio, P. F.; Baker, G. A.; Veith, G. M.; Unocic, R. R.; Mahurin, S. M.; Chi, M. F.; Dai, S. *Chem. Commun.* **2010**, *46*, 4487–4489. (i) Coleman, J. N. *Acc. Chem. Res.* **2013**, *46*, 14–22.